Plasmon-enhanced photocatalytic hydrogen production on Au/TiO_2 hybrid nanocrystal arrays

Author links open overlay panelBao-HsienWu[a1]Wei-TingLiu[a1]Tzu-YuChen[b]Tsong-PyngPerng[a]Jer-HsingHuang[b]Lih-JuannChen[a]
Show more

https://doi.org/10.1016/j.nanoen.2016.07.029Get rights and content

Highlights

- Highly regular hexagonal close-packed core-shell Au/TiO_2 hybrid nanocrystal arrays.
- Outstanding photocatalytic properties for methanol aqueous solution splitting.
- Exceptional improvement from strong coupling of the enhanced electric field.
- FDTD simulations demonstrating lateral coupling of plasmonically enhanced field.
- Optimal structures for maximum enhancement can be designed.

Abstract

In recent years, hybrid nanostructure consisted of plasmonic metals and different dielectricshave attracted much attention for their intriguing plasmonic properties. Recent studies have also shown that by introducing plasmonic metals, the photocatalytic efficiency of semiconductor can improve via plasmon-enhanced light absorption. In this work, we have demonstrated excellent photocatalytic properties for hydrogen production using hexagonal close-packed core-shell Au/TiO_2 hybrid nanocrystal arrays. Under both ultra-violet and visible light, significant increase in the hydrogen production from methanol (20%) solution splitting was achieved with the hybrid Au/TiO_2 nanocrystal arrays in comparison with bare TiO_2 thin film as well as randomly distributed Au/TiO_2 nanocrystals. From the finite differencetime domain (FDTD) simulation, the significant increase (up to 60%) in hydrogen production

can be correlated to strong and optimum coupling of the enhanced electric field from localized surface plasmon resonance in Au/TiO_2 nanocrystal arrays. In addition to allowing more accurate measurement of plasmonic enhancement, the ordered nanostructures have been shown to be especially amenable to the systematic analysis of lateral coupling of plasmonically enhanced electric field. As a result, optimal structures with appropriate spacing of core-shell metal-dielectric nanocrystals, metal core size and dielectric shell thickness for maximum enhancement can be designed.

Graphical abstract

Under both ultra-violet and visible light, significant increase in the hydrogen production from methanol (20%) solution splitting was achieved with the hybrid Au/TiO_2 nanocrystal arrays in comparison with bare TiO_2 thin film as well as randomly distributed Au/TiO_2 nanocrystals.

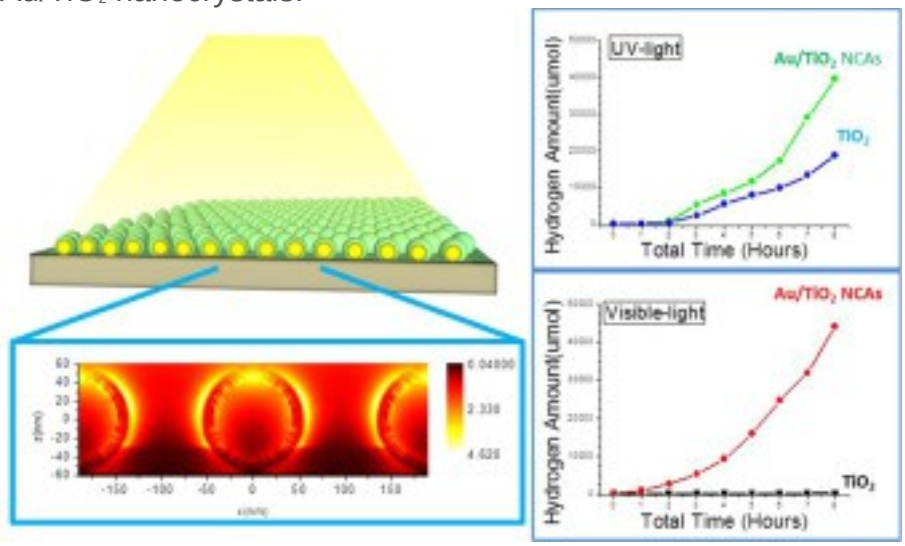

1. Download high-res image (233KB)
2. Download full-size image

- **Previous** article in issue
- **Next** article in issue

Keywords

Localized surface plasmon resonance
Metal nanocrystal array
Photocatalytic reactions
Hydrogen production

1. Introduction

Nowadays, various metal and semiconductor materials with intriguing plasmonic optical properties attracted much attention. The tremendous progresses in precise control of the shape, size, morphology and distribution of nanocrystals have made those localized surface plasmon resonance (LSPR) properties more amenable for analysis and fundamental understanding [1], [2], [3]. In particular, a previous work showed that the LSPR wavelengths of the Au nanocrystal arrays (NCAs) could be systematically tuned from the visible to near-infrared region by controlling the diameter of the Au nanocrystals and immersion of Au nanocrystals in silicon [2], [4].

However, to meet the requirements for various applications, hybrid nanostructure prepared by integrating plasmonic metal with different dielectrics, such as SiO_2, ZnO, Fe_3O_4, are of importance [4], [5], [6]. Compared with single-component plasmonic metal, the hybrid nanostructures exhibit extraordinary optical, electronic, and magnetic properties combining with unique LSPR properties [7], [8].

As the ubiquitous basic materials of modern electronic devices, semiconducting materialsare widely investigated. On the other hand, a number of important semiconductors are often wide-bandgap materials and interact weakly with visible-light. Thus, in order to increase the response to visible-light of the semiconductor, many bandgap engineering methods, including doping C, N, or metal elements, have been explored [9], [10]. An alternative scheme, introducing plasmonic metal to semiconductor to form hybrid metal-semiconductor nanostructure has been considered a more promising approach [11], [12], [13], [14], [15]. The increase of visible-light absorption of the hybrid nanostructure can be attributed to two origins. First, under the visible-light resonating with the LSPR of the plasmonic metal, the localized electric field near the metal/semiconductor interface is enhanced by LSPR effect, hence increasing electron-hole pairs in the semiconductor region. Second, metal component may help separate the electron-hole pairs and increase surface reactions.

Nevertheless, for the wavelength of the incident light with energy less than the bandgap of semiconductor, normally electron-hole pairs are not generated in the semiconductor. Once the incident light stimulated LSPR effect, the electron-transfer may occur in the hybrid nanostructure due to the hot electron effects [16], [17], [18]. Direct photoexcitation and plasmon decay are the two main possible hot electrons generation mechanisms. For plasmon-induced hot electrons, the transition was driven by the localized plasmon-induced near field [19], [20], [21]. The plasmonic hot electron generation is proportional to plasmon-induced near field intensity with enhancement, while occurring independently of bulk absorption [22], [23]. The plasmon-induced hot electrons generation would be efficient since the plasmonic absorbers can lead to near-

perfect absorption [24], [25]. Moreover, hot electrons generated by plasmon decay have higher energies than those by direct excitation, making plasmon-enhanced photocatalysis more efficient [26], [27].

In the present work, the Au/TiO_2 hybrid nanocrystal arrays were successfully fabricated. Combining colloidal lithography, dewetting process driven by surface energy and atomic layer deposition (ALD), a large area of hexagonal close-packed Au/TiO_2 hybrid nanocrystal arrays with 100–110 nm single crystalline Au core, 10–40 nm TiO_2 shell are prepared with highly ordered periodicity. The spacing of nanocrystal arrays can be controlled by proper selection of colloidal size, while the Au core and TiO_2 shell by the thicknesses of deposition. Through tuning the thickness of TiO_2 of the nanocrystal arrays, the LSPR wavelength can be adjusted to red shift and splitting into two LSPR peaks. The scattering spectra of the nanocrystal arrays can be interpreted by the simulated results based on Mie theory.

The hybrid Au/TiO_2 nanocrystal arrays were employed as photocatalysts in aqueous methanol solution (20%) and compared with the bare TiO_2 thin film. Under both UV and visible light, the hydrogen production efficiency of the hybrid Au/TiO_2 nanocrystal arrays exhibited significant increase in the aqueous methanol solution splitting. From the finite difference time domain (FDTD) simulation, it is seen that the electric field in TiO_2 has been significantly enhanced by LSPR, confirming that the generation of electron and hole pairs was increased by plasmon-enhanced light absorption.

In addition, the regular spacing of NCAs affected the efficiency of hydrogen production compared to the randomly distributed Au/TiO_2 particles. The significant lateral electric field coupling in periodical NCAs may reinforce the electric field constructively, while the lateral coupling has been impaired with random core-to-core spacings. Furthermore, the near-field enhancement was found to increase with the size of Au core, which led to stronger lateral electric field coupling as well as higher photocatalytic efficiency.

2. Experimental

2.1. Fabrication of the hexagonal Au/TiO_2 hybrid nanocrystal arrays

The hexagonal close-packed Au/TiO_2 hybrid nanocrystal arrays were fabricated in two steps: the fabrication of hexagonal Au nanocrystal arrays and the deposition of TiO_2 by atomic layer deposition.

For the formation of Au nanocrystal arrays, the monolayer polystyrene spheres (PS spheres) were spread on the sodium dodecyl sulfate decorated glass substrates, then immersed into deionized water gradually. The monolayer was scooped up with a clean Si substrate. With appropriate power and time, the size of the PS spheres was

controlled with O_2 plasma etching. The SiO_2 layer of different thickness was then deposited at a rate of 0.05 nm/s on the monolayer PS spheres arrays with an electron beam evaporation system under 10^{-6} Torr. To remove PS spheres and obtain the SiO_2 honeycomb cells arrays, samples were soaked in toluene with ultrasonic vibration for 5 h. Subsequently, the Au film was deposited on SiO_2 honeycomb cell arrays by electron beam deposition with various thicknesses at a rate of 0.1 nm/s under a vacuum of 10^{-6} Torr. The as-deposited samples were annealed in a quartz tube furnace at 1000 °C for 10 min in Ar atmosphere. The metal films were dewetted and formed hexagonal Au nanocrystal arrays..
After the colloidal lithography and the annealing process, TiO_2 layers of different thicknesses were deposited by atomic layer deposition. With tetrakis-dimethylamino titanium (TDMAT) as the precursor, the deposition cycle was set as 1 s/5 s/3 s/5 s at 0.057 nm/cycle. The hexagonal Au/TiO_2 hybrid nanocrystal arrays were then successfully fabricated.

2.2. Measurements of the scattering spectra

The normalized scattering spectra of nanocrystal arrays were measured by far-field optical spectroscopy. A 100 W halogen lamp was used as the excitation source. The light from the source was focused and incident on the sample through a 100× (N.A.=0.95) objective lens by dark-field illumination. With the diameter of the collection region being 2 mm, the scattered light was collected by the same objective lens and was transmitted into a spectrometer (BTC 111E, B&W tec, USA) with an optical fiber. The obtained spectra were subjected to proper boxcar smoothing and intensity normalization, and the background signal was all subtracted.

2.3. Measurement of the Hydrogen production by gas chromatography

In the photocatalytic experiment, the Au/TiO_2 nanocrystal arrays (1 cm×1 cm) were utilized as the photocatalysts with various TiO_2 thickness or Au sizes in a 1:4 v/v methanol/aqueous solution. The solution and the catalysts were transferred into a cylindrical reactor connected to gas chromatography system (Shimadzu GC-2014, the whole volume is 65 ml, equipped with a gas inlet valve and a gas outlet valve.). Purged with Ar for 1 h, the reactor was tightly closed. The irradiation source was a 200 W Hg lamp as the UV light source, while a 150 W Xe lamp was utilized as the visible light source. Both lamps irradiated with a distance of 5 cm between the light source and the surface of the reactor.

3. Results and discussion

Fig. 1 schematically illustrates the fabrication sequence of Au/TiO_2 hybrid nanocrystalarrays. The whole fabrication process can be divided into two steps: the fabrication of hexagonal Au nanocrystal arrays and the deposition of TiO_2 by atomic layer deposition.

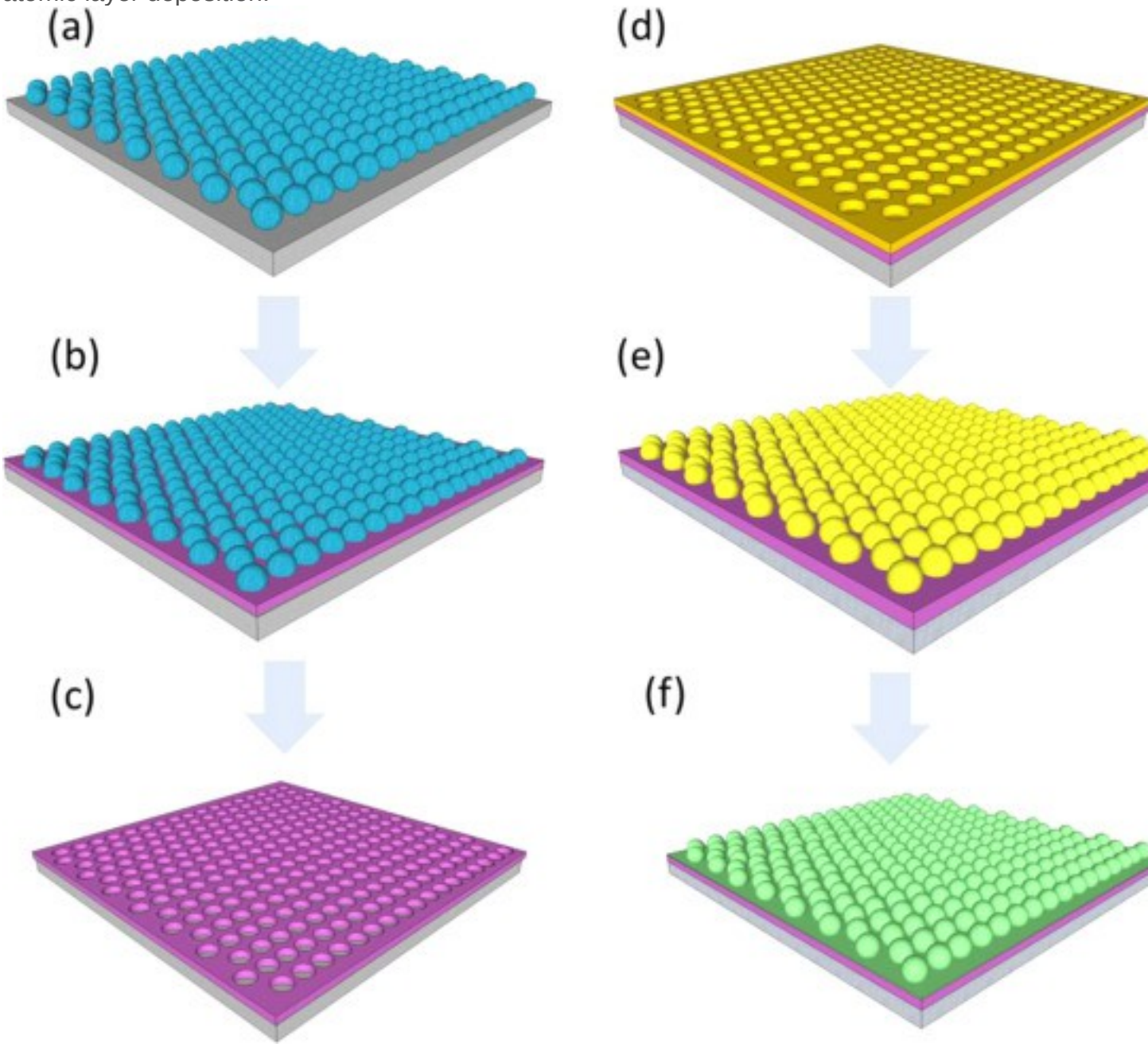

1. Download high-res image (690KB)
2. Download full-size image

Fig. 1. Fabrication sequence diagrams of the hexagonal Au/TiO_2 hybrid nanocrystal arrays: (a) arrangement of monolayer polystyrene (PS)

spheres; (b) deposition of SiO_2 layer; (c) removal of the PS spheres; (d) deposition of Au film; (e) annealing to form the close-packed Au nanocrystal arrays; (f) deposition of TiO_2 by atomic layer deposition.

For the formation of Au nanocrystal arrays, the monolayer polystyrene spheres were first dispersed on a clean Si substrate as the mask to define the nanocrystal arrays. After O_2plasma etching, the hexagonal SiO_2 layer was deposited by an electron beam evaporation system to form the honeycomb walls. Then the PS spheres were removed with the SiO_2layer remained, followed by the deposition of the Au film. With SiO_2 network serving as separation ridges, the Au nanocrystal arrays were formed during the annealing process. (Fig. 1**a~e**) In our previous work, the Au nanocrystals were found to be single crystalline, which is beneficial to LSPR properties for the internal losses derived by plasmons scattering at grain boundaries would be avoided and the maximal near-field intensity enhancement would be reached [2].

After the colloidal lithography and the annealing process, TiO_2 layer was deposited by atomic layer deposition (ALD). Atomic layer deposition is well-known for excellent step coverage, uniform deposited film and high precision film thickness. Those advantages contributed to the surface reaction mechanism of chemisorption saturation and self-limiting film growth, differing from the traditional deposition technology. Furthermore, the TiO_2 layers coated by ALD were analyzed to be amorphous. (See the Supporting Information, **S1**) With the localized electronic states due to the structural disorder inside the bandgap, the amorphous TiO_2 are more likely to increase the absorption [17].

By separately introducing the precursors into the chamber, the TiO_2 film thickness can be precisely controlled. It is known that the LSPR wavelength and localized electric field enhancement are highly dependent on the surrounding media. The top view SEM images are shown in Fig. 2. (Cross-section TEM image is shown in S2) Fig. 2**a** shows a low magnification SEM image revealing ordered periodicity of Au nanocrystal arrays over a relatively large area. In Fig. 2**b**, it can be seen that the Au particles are located at the middle of the honeycomb SiO_2 walls. In Figs. 2**c** and **d**, it is clear that the TiO_2 shells coated by ALD were uniformly distributed on the Au nanocrystal arrays, and the thickness of the TiO_2 shell is nearly the same. In addition, the periodicity of the Au nanocrystal arrays was maintained after the ALD deposition process.

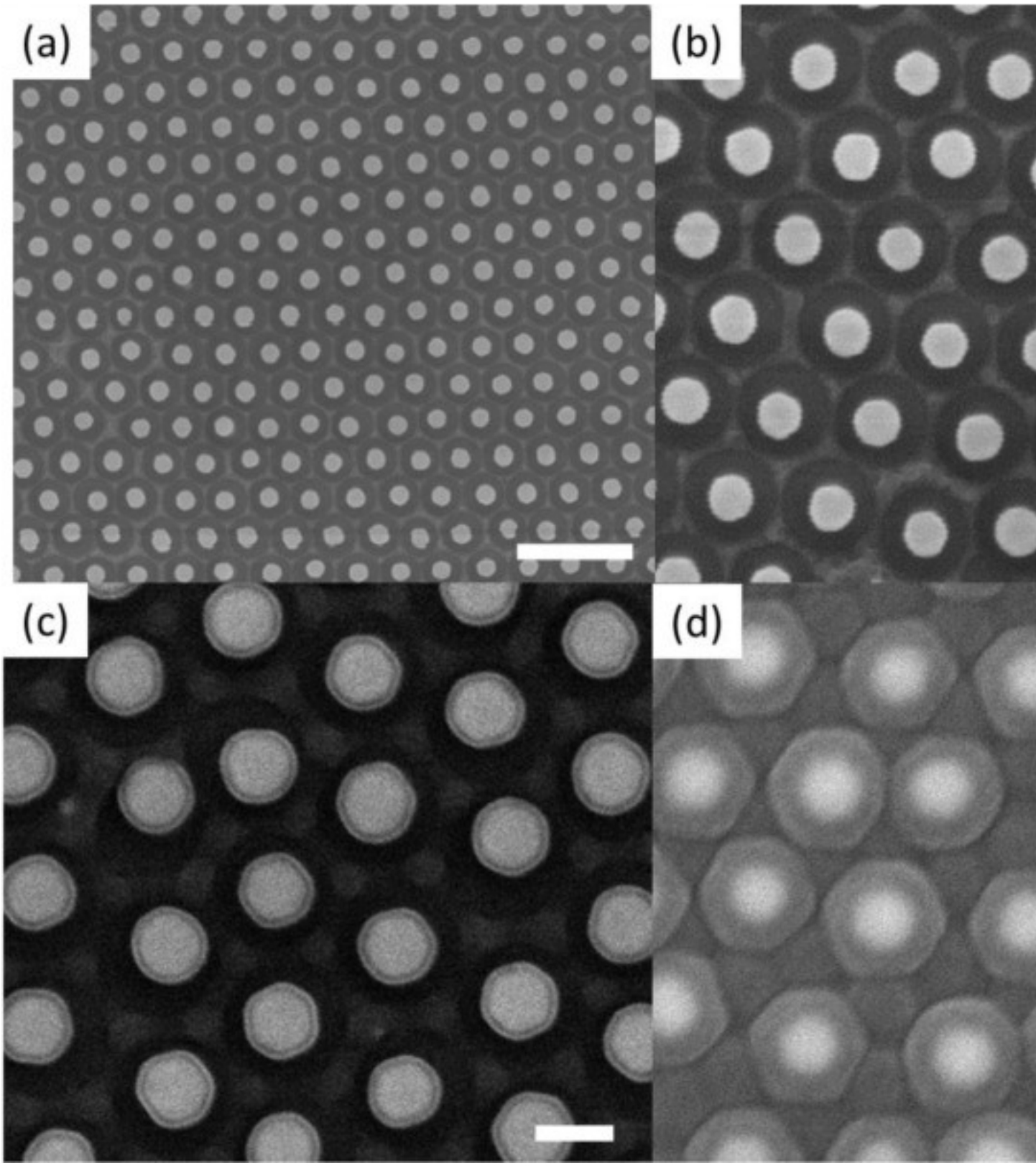

1. Download high-res image (1024KB)
2. Download full-size image

Fig. 2. Top view SEM images of the hexagonal close-packed nanocrystal arrays: (a) low magnification (with the scale bar corresponding to 500 nm) and (b) high magnification images; (c) 10 nm TiO_2/Au (shell/core) deposited by ALD; (d) 40 nm TiO_2/Au (shell/core) deposited by ALD. The scale bars in (b)-(d) correspond to 100 nm.

It is known that the wavelength and intensity of LSPR depend on the morphology of the nanostructures and local dielectric environment [1], [2]. Fig. 3**a** shows the simulation of scattering spectra of Au nanocrystal arrays with different surrounding media based on Mie's theory. The extinction, scattering and absorption efficiencies can all be considered in the simulations. To simplify the simulations, spherical nanocrystal was assumed and coupling effect was neglected. The normalized measured scattering spectra of nanocrystal arrays by far-field optical spectroscopy are shown in Fig. 3**b**. A 100 W halogen lamp was used as the excitation source. The detailed measurement method and simulation has been reported in our previous paper and are described in S3[2], [28]. The background signal had already been subtracted from the spectra. The LSPR wavelengths (λ_{LSPR}) are marked in the figure. These nanocrystal arrays exhibit λ_{LSPR} in the range of 500–650 nm. The λ_{LSPR} of bare Au nanocrystal arrays is about 575 nm, which agrees with that of our previous work [2]. After deposition of 10 nm TiO_2, two λ_{LSPR} peaks, 540 nm and 620 nm, were found. The splitting of the peaks can be explained by Mie theory since the Au in Au/TiO_2 nanocrystal arrays were only encircled partly by TiO_2 and partly by SiO_2. As a result, the scattering may result in two peaks located near 521 nm and between 606 nm and 675 nm, which are in agreement with experimental findings.

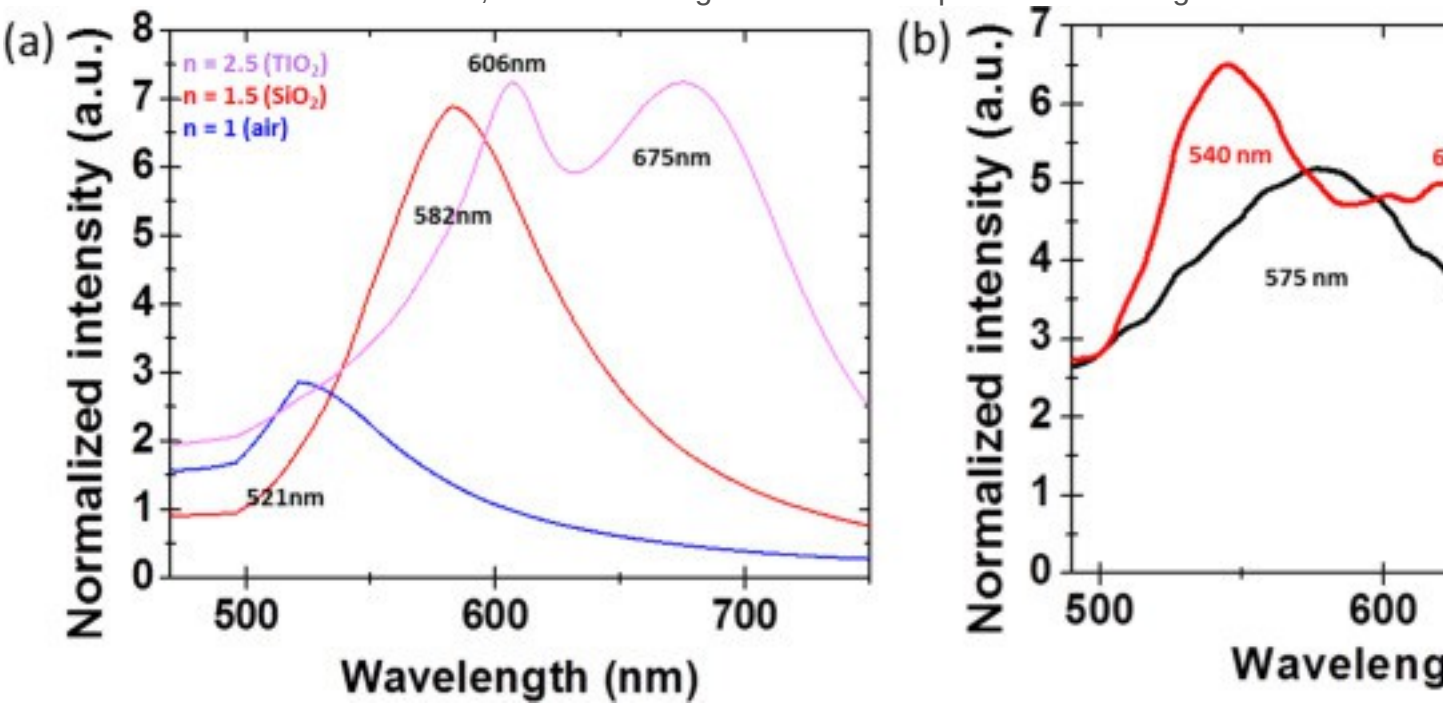

1. Download high-res image (348KB)
2. Download full-size image

Fig. 3. (a) Simulated scattering spectra for Au nanocrystal arrays with crystal size of 100 nm in different surrounding media: TiO_2, SiO_2 and air. (b) Measured scattering spectra for Au nanocrystal arrays with Au size of 100 nm and Au/TiO_2 nanocrystal arrays with 10 nm TiO_2. A 100 W halogen lamp was used as the excitation source.

The photocatalytic properties of the Au/TiO_2 nanocrystal arrays were investigated with a 1:4 v/v methanol/aqueous solution. The hydrogen production results under UV-light irradiation are shown in Fig. 4**a**. Compared to those with bare TiO_2 film, Au/TiO_2 nanocrystal arrays display significantly higher photocatalytic activities. From Table S1, for both 10 and 40 nm TiO_2 films, the hydrogen production rates increase substantially with the presence of Au/TiO_2 NCAs. The occurrence of the plasmon enhanced electric field in Au particles improves the probability of the generation of the electron-hole pairs. In addition, the electrons generated in TiO_2 move to Au regions, which also act as catalytic sites, thus prolong the lifetime of the electron and hole pairs. In Fig. 5**a**, FDTD simulation shows the near-field was increased by 3 times from the injected UV-light. Furthermore, although the hydrogen production rate increases as the TiO_2 thickness increases, the plasmon photocatalytic enhancement is more obvious for 10 nm TiO_2 (175%) than 40 nm TiO_2(117%). It is likely due to exponential decay of the plasmon enhanced near-field in TiO_2 from the Au/TiO_2 interface.

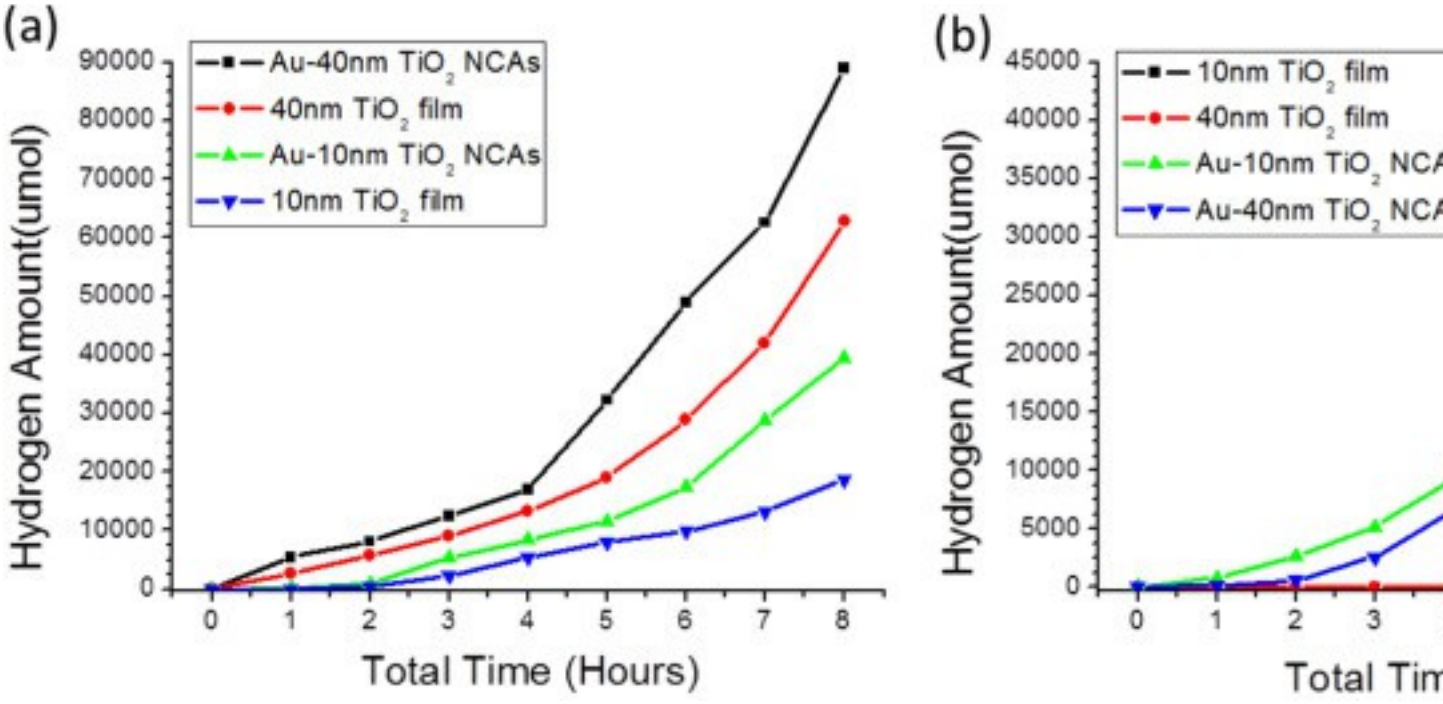

1. Download high-res image (389KB)
2. Download full-size image

Fig. 4. Amount of hydrogen generated with samples of different coating thickness of TiO_2 forming Au/TiO_2NCAs as photocatalysts compared with bare TiO_2 thin films under (a) UV-light irradiation (Hg lamp) and (b) visible-light irradiation (Xe lamp).

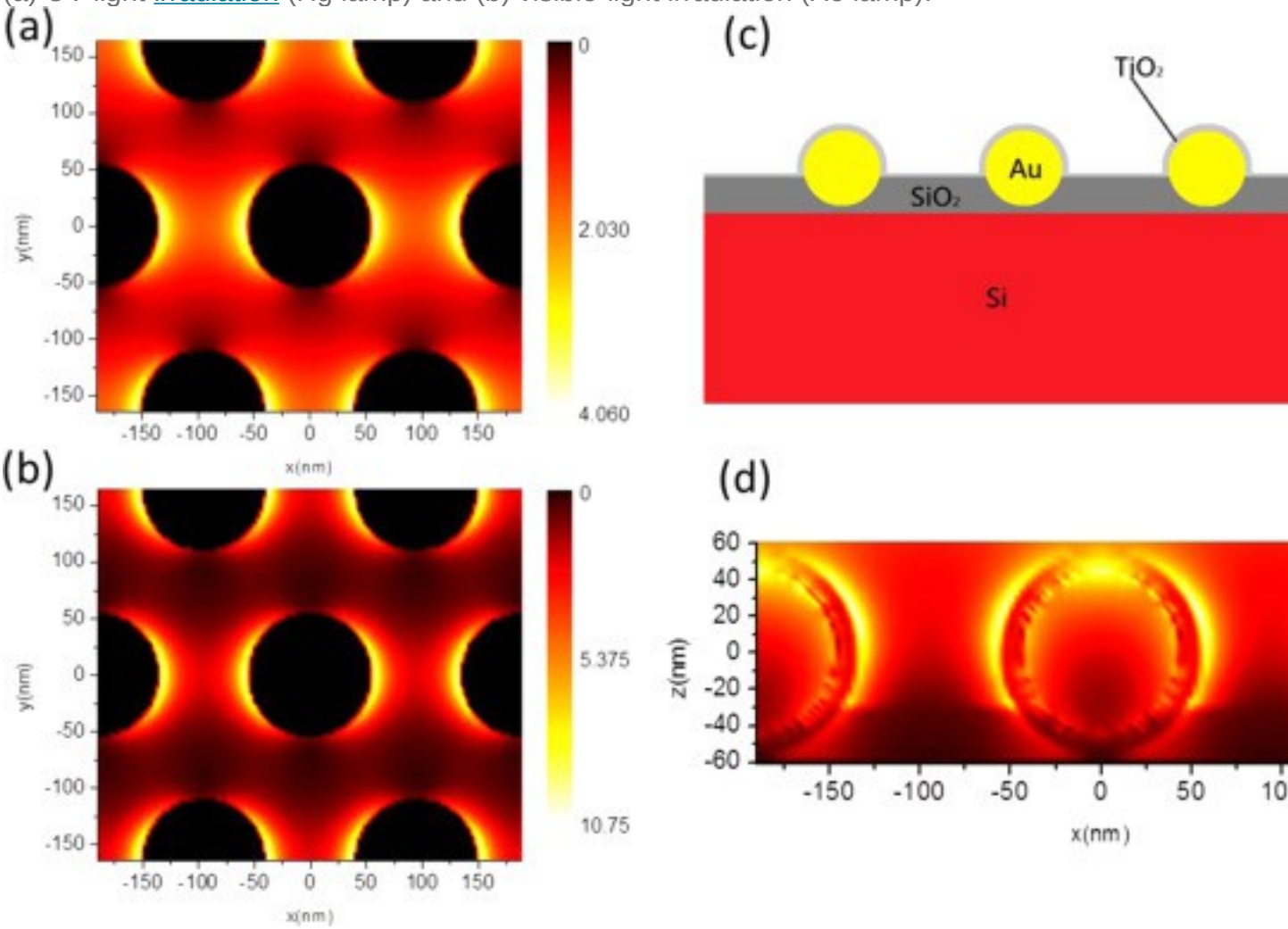

1. Download high-res image (498KB)
2. Download full-size image

Fig. 5. The mappings of electric near-fields simulated by finite difference time domain method for Au-10 nm TiO_2 nanocrystal arrays under different wavelengths polarized along x-axis, (a) 380 nm and (b) 620 nm. (c) Schematic diagram of cross-section of the Au/TiO_2 nanocrystal arrays. (d) The mapping of cross-section near-fields for Au-10 nm TiO_2 nanocrystal arrays partially immersed in SiO_2 simulated by FDTD, λ=540 nm.

On the other hand, the photocatalytic activities of the bare TiO_2 thin films of different thicknesses (10 and 40 nm) were at very low level under visible-light irradiation (cutoff filter, λ<440 nm) as shown in Fig. 4**b**. It can be understood that the direct

photoexcitation of TiO_2occurs only when the energy of the injecting photons is higher than the bandgap of TiO_2, that is, $\lambda<380$ nm. Consequently, visible-light irradiation of the TiO_2 thin film results in very low level hydrogen production.

In contrast, for Au/TiO_2 NCAs, the visible-light irradiation can stimulate the generation of the electron-hole pairs in TiO_2. Fig. 4**b** shows that the Au/TiO_2 NCAs induced high photocatalytic activities. Furthermore, the photocatalytic activity of Au/10 nm TiO_2 NCAs is higher than that of Au/40 nm TiO_2 NCAs. It is thought that, under visible-light irradiation, not only the excitation of the LSPR takes place, but the surface plasmon excitations under the enhanced plasmon near-fields close to Au/TiO_2 interface also results in the generation of hot electrons. In Fig. 5**b**, the near-field intensity is seen to increase by about 10 times. Moreover, with the corroboration of photocatalytic activity under illumination of visible-light being higher than that of UV-light, the plasmon-induced hot electrons are more efficient and have higher energies than those from direct photoexcitation [26], [27]. As the electrons migrate to the TiO_2 conduction band, the probability of recombination of the electron-hole pairs decreases. Since the plasmonic near-fields are localized close to the Au/TiO_2 interface, the increase of the thickness of TiO_2 has little influence on the effect of near-fields intensity. As a result, the photocatalytic activity of Au/10 nm TiO_2 NCAs is higher than that of Au/40 nm TiO_2 NCAs mainly due to shorter distance for migration of electrons in thinner TiO_2. Accordingly, in thicker TiO_2 layer, the recombination is more prone to occur; hence the photocatalytic activity is lower.

On the other hand, the surrounding dielectric media also play an important role in the enhancement of the plasmonic near-fields. From the cross-section structure of the Au/TiO_2NCAs illustrated in Fig. 5**c**, it can be seen that a non-symmetric structure encloses the Au nanoparticles with the upper and lower surroundings being TiO_2 and SiO_2, respectively. The FDTD near-fields intensity simulation is shown in Fig. 5**d**. It is obvious that the near-field intensity in TiO_2 is greater than in SiO_2. It is the difference in dielectrics in surrounding media (SiO_2 refractive index=1.5, TiO_2 refractive index=2.5) that made the near-field intensity distribution asymmetric and concentrated in TiO_2[17].

To investigate whether the regular spacing of NCAs affected the efficiency of hydrogen production compared to the randomly distributed Au/TiO_2 particles, further photocatalytic measurements were carried out. The morphology of the randomly distributed Au NPs is shown in the inset of Fig. 6. With significant variation in size of Au cores and different core-to-core spacings, the Au/TiO_2 nanocomposites exhibit no apparent periodicity. Fig. 6 shows that for samples with the presence of Au/TiO_2 NCAs, higher photocatalyic activities occur than those with randomly distributed Au/TiO_2 nanocomposites.

From Table S2, considering randomly distributed Au/TiO_2 core-shell structure, the Au part still enhances TiO_2 surface electric field due to LSPR, the lateral coupling between neighboring Au particles has been less efficient with varied core-to-core spacings. In contrast, for Au/TiO_2 NCAs, not only the electric field is enhanced at interfaces along all directions, but the lateral coupling also accentuated the enhancement significantly, as evident in the simulated image shown in Fig. 5.

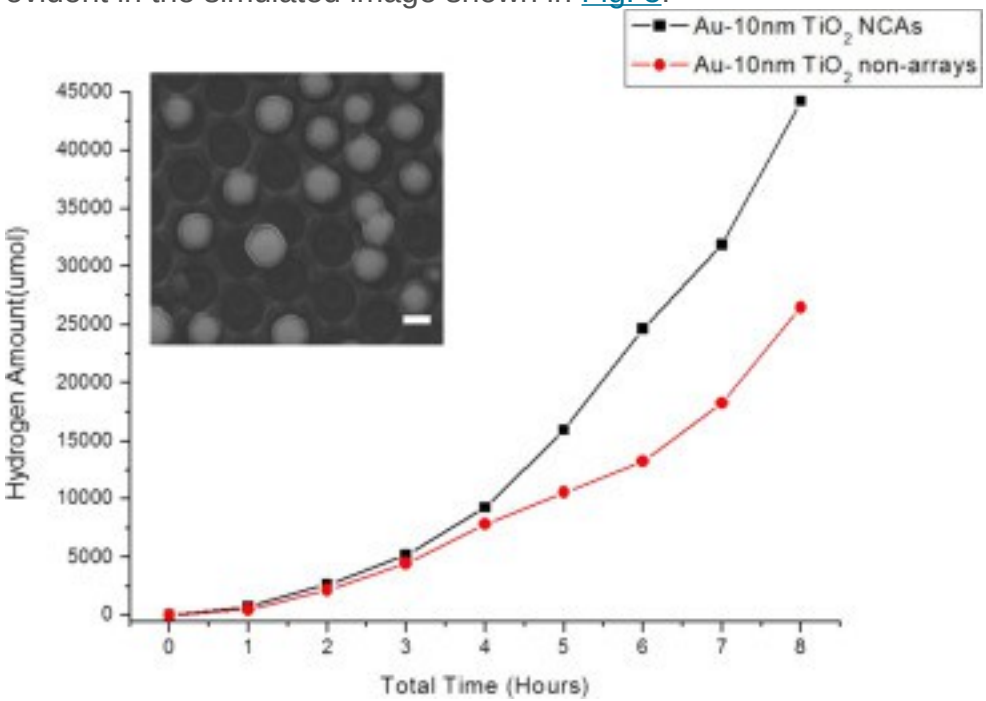

1. Download high-res image (155KB)
2. Download full-size image

Fig. 6. Amount of hydrogen produced from Au/TiO_2 NCAs and randomly distributed Au/TiO_2 nanoparticleswith the same thickness of TiO_2 under visible light irradiation. Inset is the SEM image of randomly distributed Au/TiO_2 nanoparticles. The scale bar corresponds to 100 nm.

Since the well-arranged core-to-core spacing of the Au/TiO_2 NCAs does influence the electric field distribution, enlarging the Au core with the same spacing may increase the plasmon-enhancement of the near-field.

Fig. 7**a** and Table S3 show the amount of hydrogen generated from Au/TiO_2 NCAs with the same thickness of TiO_2 (10 nm) but different sizes of Au core (110 nm and 100 nm) under visible light irradiation. Inset is the SEM image of 110 nm Au core/TiO_2 NCAs. It is apparent that with the same TiO_2 thickness, the larger the Au core, the higher the H_2 production efficiency. Fig. 7**b** shows calculated cross-section near-field distribution with lateral coupling. The electric field intensity is enhanced up to 6.4 times, instead of

4.6 times for 100 nm Au/TiO_2 NCAs shown in Fig. 5**d**. Accordingly, the photocatalytic efficiency of 110 nm Au/TiO_2NCAs increases by about 16.67%. The results indicated that with larger Au core, hence closer distance between Au nanoparticles, stronger coupling between neighboring nanoparticles led to higher plasmon-enhanced photocatalyic activities.

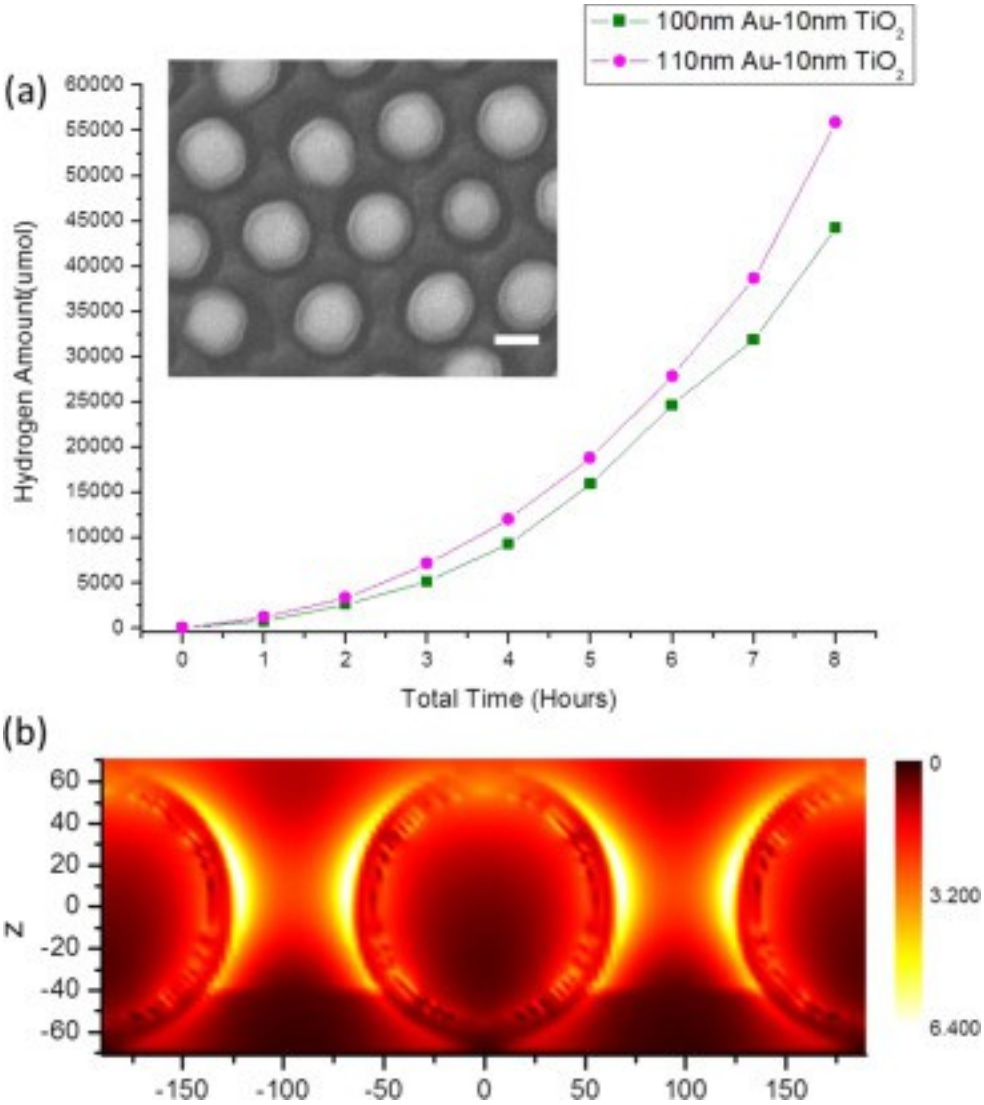

1. Download high-res image (356KB)
2. Download full-size image

Fig. 7. (a) Amount of hydrogen generated from Au/TiO_2 NCAs with the same thickness (10 nm) of TiO_2but larger Au core (110 nm) under visible light irradiation. Inset is the SEM image of 110 nm Au core /TiO_2NCAs. The scale bar corresponds to 100 nm. (b) The mapping of cross-section near-fields simulated by FDTD method, λ=550 nm.

Moreover, to explore further the plasmonic resonance behavior of the enlarged Au core, we have carried out a series of near field simulations by FDTD. The mapping of cross-

section near field with the size of the Au core being 120, 130, 140 and 150 nm and with peaks of the scattered spectra λ=560, 570, 580 and 590 nm, respectively, indicates the red shift of LSPR peaks with the enlarged Au core [2]. As shown in Fig. 8, the maximum intensity of the near field was increased from 9.2 times for the 120 nm Au cores to 18.9 times for the 150 nm Au cores, indicating that the lateral coupling was enhanced remarkably as the size of Au core increased. Therefore, with a greater lateral coupling, the photocatalyic activity would be significantly enhanced.

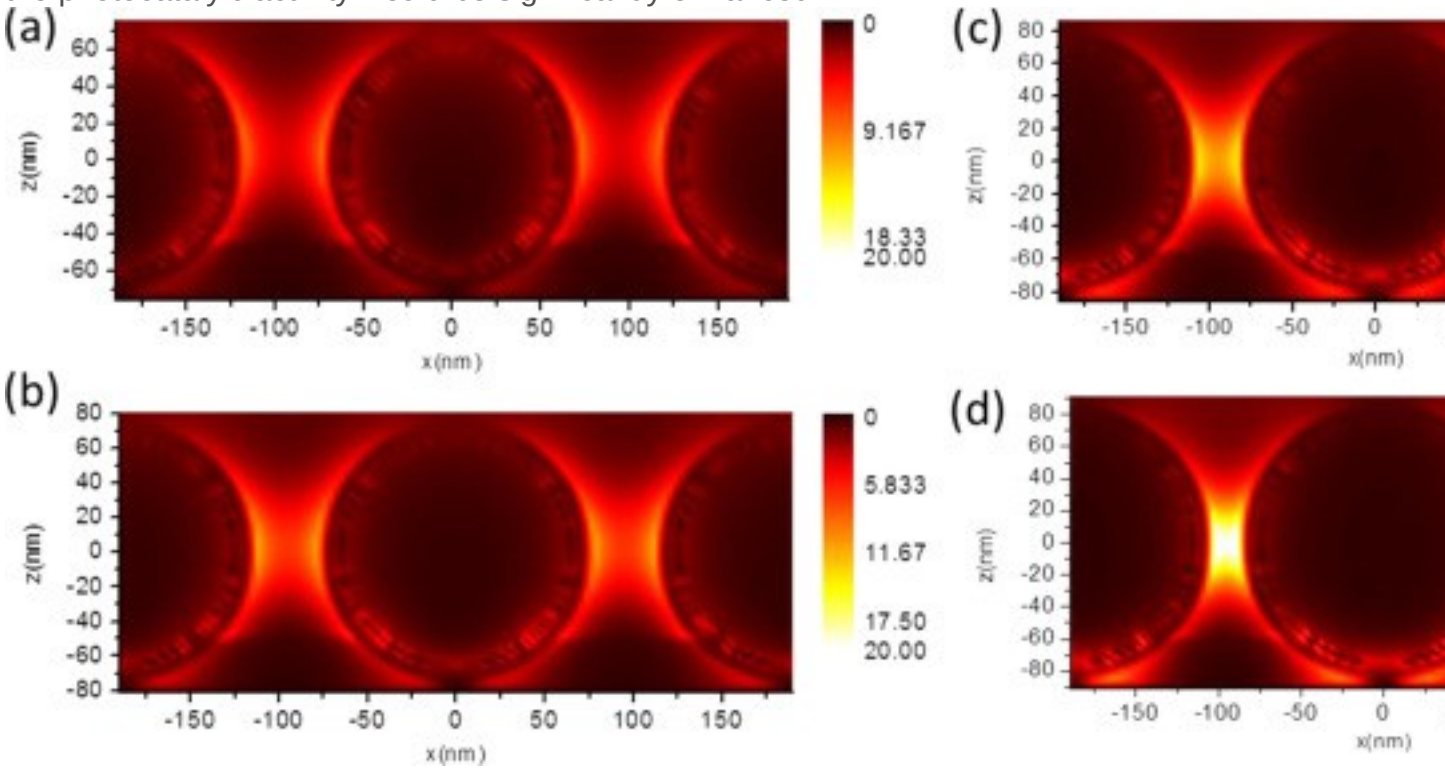

1. Download high-res image (471KB)
2. Download full-size image

Fig. 8. The mappings of cross-section near-fields simulated by FDTD method, the size of the Au core are (a) 120, (b) 130, (c) 140 and (d) 150 nm, with peaks of the scattered spectra λ=560, 570, 580 and 590 nm, respectively. To emphasize the enhanced near-field intensity, the contrast of the color scale was adjusted to be in the same range, with the maximum intensity being 9.2, 11.75, 14.4, 18.9, respectively.

Table S4 lists the comparison of present results with reported data in the literatures for Au-TiO_2 system and some other catalysts [29], [30], [31], [32], [33], [34], [35], [36]. Although the hydrogen production rate may vary significantly with the water/methanol ratio, intensity of the irradiation source, experimental set-up etc. The photocatalytic performance of Au-10 nm TiO_2 NCAs stands out as remarkably high. The results

indicate that the plasmonic photocatalytic enhancement is very effective with the well-designed metal/semiconductor hybrid structure.

4. Conclusions

In conclusion, we have successfully fabricated the hybrid Au/TiO_2 nanocrystal arrays with highly ordered periodicity and uniformity. Under both ultra-violet and visible light, significant increase in the hydrogen production from methanol (20%) solution splitting was achieved with the hybrid Au/TiO_2 nanocrystal arrays in comparison with bare TiO_2 thin film as well as randomly distributed Au/TiO_2 nanocrystals. With larger refractive index TiO_2 as the surrounding dielectrics, the LSPR of the Au/TiO_2 nanocrystal arrays red-shifts. With the strong localized plasmonic near-field enhancement at the Au/TiO_2 interface, the photocatalytic efficiencies increase under both UV-light and visible-light. On the other hand as the thickness of TiO_2 increased from 10 to 40 nm, the photocatalytic efficiency under visible-light irradiation decreased instead for the carrier recombination is more prone to occur in thicker TiO_2 layer. From the data of photocatalyic activities, the plasmon-induced hot electrons were found to be more efficient, compared to those from direct photoexcitation.
Furthermore, the lateral coupling has been systematically investigated for the first time. Owing to the highly ordered periodicity, the lateral coupling of the electric field is shown to be more significant compared to the randomly distributed Au/TiO_2 nanocrystals, hence higher photocatalytic activity, as obtained from both theoretical calculations and experimental findings. The Au core size and the TiO_2 shell thickness are also shown to affect the photocatalytic activities. The results are particularly useful in designing of optimal structures of regular metal-dielectric nanocrystals with appropriate spacing of nanocrystals, metal core size and dielectric shell thickness.

Notes

The authors declare no competing financial interests.

Acknowledgments

We are grateful to late Prof. Li-Jen Chou for helpful discussion. The research was sponsored by the Ministry of Science and Technology of Taiwan under grant no. MOST 104-2221-E-007-30-MY3.

Appendix A. Supplementary material

Download Word document (567KB)Help with docx files

Supplementary material **Supporting Information**. Characterization of ALD-deposited TiO_2, cross-section TEM images and Fig. S1–S4 are available in the supporting information. This material is available free of charge via the Internet at

References

[1]

H.J. Chen, X.S. Kou, Z. Yang, W.H. Ni, J.F. Wang**Shape- and size-dependent refractive index sensitivity of gold nanoparticles**

Langmuir, 24 (10) (2008), pp. 5233-5237

CrossRefView Record in Scopus

[2]

H.W. Ting, Y.K. Lin, Y.J. Wu, L.J. Chou, C.J. Tsai, L.J. Chen**Large area controllable hexagonal close-packed single-crystalline metal nanocrystal arrays with localized surface plasmon resonance response**

J. Mater. Chem C, 1 (22) (2013), pp. 3593-3599

CrossRefView Record in Scopus

[3]

G.J. Lin, H.P. Wang, D.H. Lien, P.H. Fu, H.C. Chang, C.H. Ho, C.A. Lin, K.Y. Lai, J.H. He**A broadband and omnidirectional light-harvesting scheme employing nanospheres on Si solar cells**

Nano Energy, 6 (2014), pp. 36-43

ArticleDownload PDFView Record in Scopus

[4]

Y.K. Lin, H.W. Ting, C.Y. Wang, S. Gwo, L.J. Chou, C.J. Tsai, L.J. Chen**Au nanocrystal array/silicon nanoantennas as wavelength-selective photoswitches**

Nano Lett., 13 (6) (2013), pp. 2723-2731

CrossRefView Record in Scopus

[5]

M. Mahanti, D. Basak**Highly enhanced UV emission due to surface plasmon resonance in Ag-ZnO nanorods**

Chem. Phys. Lett., 542 (2012), pp. 110-116

ArticleDownload PDFView Record in Scopus

[6]

Y.X. Zhang, H.L. Ding, Y.Y. Liu, S.S. Pan, Y.Y. Luo, G.H. Li**Facile one-step synthesis of plasmonic/magnetic core/shell nanostructures and their multifunctionality**

J. Mater. Chem., 22 (21) (2012), pp. 10779-10786

CrossRefView Record in Scopus

[7]

R.B. Jiang, B.X. Li, C.H. Fang, J.F. Wang**Metal/semiconductor hybrid nanostructures for plasmon-enhanced applications**
Adv. Mater., 26 (31) (2014), pp. 5274-5309
CrossRefView Record in Scopus

[8]
G.V. Naik, V.M. Shalaev, A. Boltasseva**Alternative plasmonic materials: beyond gold and silver**
Adv. Mater., 25 (24) (2013), pp. 3264-3294
CrossRefView Record in Scopus

[9]
J.H. Park, S. Kim, A.J. Bard**Novel carbon-doped TiO_2 nanotube arrays with high aspect ratios for efficient solar water splitting**
Nano Lett., 6 (1) (2006), pp. 24-28
CrossRefView Record in Scopus

[10]
Q.J. Xiang, J.G. Yu, M. Jaroniec**Nitrogen and sulfur co-doped TiO_2 nanosheets with exposed {001} facets: synthesis, characterization and visible-light photocatalytic activity**
Phys. Chem. Chem. Phys., 13 (11) (2011), pp. 4853-4861
CrossRefView Record in Scopus

[11]
S. Linic, P. Christopher, D.B. Ingram**Plasmonic-metal nanostructures for efficient conversion of solar to chemical energy**
Nat. Mater., 10 (12) (2011), pp. 911-921
CrossRefView Record in Scopus

[12]
W.B. Hou, S.B. Cronin**A review of surface plasmon resonance-enhanced photocatalysis**
Adv. Funct. Mater., 23 (13) (2013), pp. 1612-1619
CrossRefView Record in Scopus

[13]
H.Y. Hwang, Y. Iwasa, M. Kawasaki, B. Keimer, N. Nagaosa, Y. Tokura**Emergent phenomena at oxide interfaces**
Nat. Mater., 11 (2) (2012), pp. 103-113
CrossRefView Record in Scopus

[14]

H.P. Wang, K. Sun, S.Y. Noh, A. Kargar, M.L. Tsai, M.Y. Huang, D.L. Wang, J.H. He**High-performance a-Si/c-Si Heterojunction Photoelectrodes for Photoelectrochemical Oxygen and Hydrogen Evolution**
Nano Lett., 15 (5) (2015), pp. 2817-2824
CrossRefView Record in Scopus
[15]

H.P. Wang, D.H. Lien, M.L. Tsai, C.A. Lin, H.C. Chang, K.Y. Lai, J.H. He**Photon management in nanostructured solar cells**
J. Mater. Chem C, 2 (17) (2014), pp. 3144-3171
CrossRefView Record in Scopus
[16]

C.G. Silva, R. Juarez, T. Marino, R. Molinari, H. Garcia**Influence of excitation wavelength (uv or visible light) on the photocatalytic activity of titania containing gold nanoparticles for the generation of hydrogen or oxygen from water**
J. Am. Chem. Soc., 133 (3) (2011), pp. 595-602
View Record in Scopus
[17]

Z.W. Seh, S.H. Liu, M. Low, S.Y. Zhang, Z.L. Liu, A. Mlayah, M.Y. Han**Janus Au-TiO_2 photocatalysts with strong localization of plasmonic near-fields for efficient visible-light hydrogen generation**
Adv. Mater., 24 (17) (2012), pp. 2310-2314
CrossRefView Record in Scopus
[18]

A.V. Puga, A. Forneli, H. Garcia, A. Corma**Production of H-2 by ethanol photoreforming on Au/TiO_2**
Adv. Funct. Mater., 24 (2) (2014), pp. 241-248
CrossRefView Record in Scopus
[19]

F.M. Wang, N.A. Melosh**Plasmonic energy collection through hot carrier extraction**
Nano Lett., 11 (12) (2011), pp. 5426-5430
CrossRefView Record in Scopus
[20]

Y.K. Lee, C.H. Jung, J. Park, H. Seo, G.A. Somorjai, J.Y. Park**Surface plasmon-driven hot electron flow probed with metal-semiconductor nanodiodes**
Nano Lett., 11 (10) (2011), pp. 4251-4255
CrossRefView Record in Scopus
[21]

H. Chalabi, D. Schoen, M.L. Brongersma**Hot-electron photodetection with a plasmonic nanostripe antenna**

Nano Lett., 14 (3) (2014), pp. 1374-1380
CrossRefView Record in Scopus

[22]

B.Y. Zheng, H.Q. Zhao, A. Manjavacas, M. McClain, P. Nordlander, N.J. Halas**Distinguishing between plasmon-induced and photoexcited carriers in a device geometry**
Nat. Commun., 6 (2015)

[23]

M.L. Brongersma, N.J. Halas, P. Nordlander**Plasmon-induced hot carrier science and technology**
Nat. Nanotechnol., 10 (1) (2015), pp. 25-34
CrossRefView Record in Scopus

[24]

N. Liu, M. Mesch, T. Weiss, M. Hentschel, H. Giessen**Infrared perfect absorber and its application as plasmonic sensor**
Nano Lett., 10 (7) (2010), pp. 2342-2348
CrossRefView Record in Scopus

[25]

W. Li, J. Valentine**Metamaterial perfect absorber based hot electron photodetection**
Nano Lett., 14 (6) (2014), pp. 3510-3514
CrossRefView Record in Scopus

[26]

R. Sundararaman, P. Narang, A.S. Jermyn, W.A. Goddard, H.A. Atwater**Theoretical predictions for hot-carrier generation from surface plasmon decay**
Nat. Commun., 5 (2014)

[27]

A. Manjavacas, J.G. Liu, V. Kulkarni, P. Nordlander**Plasmon-induced hot carriers in metallic nanoparticles**
ACS Nano, 8 (8) (2014), pp. 7630-7638
CrossRefView Record in Scopus

[28]

Y.J. Wu, C.H. Hsieh, P.H. Chen, J.Y. Li, L.J. Chou, L.J. Chen**Plasmon resonance spectroscopy of gold-in-gallium oxide peapod and core/shell nanowires**
ACS Nano, 4 (3) (2010), pp. 1393-1398
CrossRefView Record in Scopus

[29]

X.G. Meng, Q. Yu, T. Wang, G.G. Liu, K. Chang, P. Li, L.Q. Liu, J.H. Ye**Exceptional enhancement of H-2 production in alkaline environment over plasmonic Au/TiO_2photocatalyst under visible light**
APL Mater., 3 (10) (2015)

[30]

P.A. Bharad, K. Sivaranjani, C.S. Gopinath**A rational approach towards enhancing solar water splitting: a case study of Au-RGO/N-RGO-TiO_2**

Nanoscale, 7 (25) (2015), pp. 11206-11215

CrossRefView Record in Scopus

[31]

G.P. Singh, K.M. Shrestha, A. Nepal, K.J. Klabunde, C.M. Sorensen**Graphene supported plasmonic photocatalyst for hydrogen evolution in photocatalytic water splitting**

Nanotechnology, 25 (26) (2014)

[32]

T.F. Yeh, J.M. Syu, C. Cheng, T.H. Chang, H.S. Teng**Graphite oxide as a photocatalyst for hydrogen production from water**

Adv. Funct. Mater., 20 (14) (2010), pp. 2255-2262

CrossRefView Record in Scopus

[33]

F.L. Wang, Y.J. Jiang, D.J. Lawes, G.E. Ball, C.F. Zhou, Z.W. Liu, R. Amal**Analysis of the promoted activity and molecular mechanism of hydrogen production over fine Au-Pt alloyed TiO_2 photocatalysts**

ACS Catal., 5 (7) (2015), pp. 3924-3931

CrossRefView Record in Scopus

[34]

A. Gallo, M. Marelli, R. Psaro, V. Gombac, T. Montini, P. Fornasiero, R. Pievo, V. Dal Santo**Bimetallic Au-Pt/TiO2 photocatalysts active under UV-A and simulated sunlight for H-2 production from ethanol**

Green. Chem., 14 (2) (2012), pp. 330-333

CrossRefView Record in Scopus

[35]

F. Gartner, S. Losse, A. Boddien, M.M. Pohl, S. Denurra, H. Junge, M. Beller**Hydrogen evolution from water/alcohol mixtures: effective in situ generation of an active Au/TiO_2catalyst**

Chemsuschem, 5 (3) (2012), pp. 530-533

CrossRefView Record in Scopus

[36]

P. Cheng, Z. Yang, H. Wang, W. Cheng, M.X. Chen, W.F. Shangguan, G.F. Ding**TiO_2-graphene nanocomposites for photocatalytic hydrogen production from splitting water**

Int J. Hydrog. Energ., 37 (3) (2012), pp. 2224-2230

ArticleDownload PDFView Record in Scopus

[1]

Bao-Hsien Wu and Wei-Ting Liu contributed equally.